Formation of n- and p-type regions in individual Si/SiO2 core/shell nanowires by ion beam doping

Berencén, Y.; Prucnal, S.; Möller, W.; Hübner, R.; Rebohle, L.; Schönherr, T.; Bilal Khan, M.; Wang, M.; Glaser, M.; Georgiev, Y. M.; Erbe, A.; Lugstein, A.; Helm, M.; Zhou, S.;

Originally published:

September 2018

Nanotechnology 29(2018), 474001-474008

DOI: https://doi.org/10.1088/1361-6528/aadfb6

Nanotechnology

Formation of n- and p-type regions in individual Si/SiO_2 core/shell nanowires by ion beam doping

To cite this article before publication: Yonder Berencén *et al* 2018 *Nanotechnology* in press https://doi.org/10.1088/1361-6528/aadfb6

IOP Publishing Nanotechnology
Nanotechnology **XX** (XXXX) XXXXXX https://doi.org/XXXX/XXXX

Formation of n- and p-type regions in individual Si/SiO_2 core/shell nanowires by ion beam doping

Y Berencén[1], S Prucnal[1], W Möller[1], R Hübner[1], L Rebohle[1], T Schönherr[1], M Bilal Khan[1], M Wang[1,3], M Glaser[2], Y M Georgiev[1,§], A Erbe[1], A Lugstein[2], M Helm[1,3] and S Zhou[1]

[1] Helmholtz-Zentrum Dresden-Rossendorf, Institute of Ion Beam Physics and Materials Research, Bautzner Landstraße 400, D-01328 Dresden, Germany
[2] Institute for Solid State Electronics, Vienna University of Technology, Floragasse 7, A-1040 Vienna, Austria
[3] Center for Advancing Electronics Dresden (cfaed), Technische Universität Dresden, 01062 Dresden, Germany
[§] On leave of absence from the Institute of Electronics at the Bulgarian Academy of Sciences, 72, Tzarigradsko chaussee blvd., 1784 Sofia, Bulgaria

E-mail: y.berencen@hzdr.de

Received xxxxxx
Accepted for publication xxxxxx
Published xxxxxx

Abstract

A method for cross-sectional doping of individual Si/SiO_2 core/shell nanowires is presented. P and B atoms are laterally implanted at different depths in the Si core. The healing of the implantation-related damage together with the electrical activation of the dopants takes place via solid phase epitaxy driven by millisecond-range flash lamp annealing. Electrical measurements through a bevel formed along the nanowire enabled us to demonstrate the concurrent formation of n- and p-type regions in individual Si/SiO_2 core/shell NWs. These results might pave the way for ion beam doping of nanostructured semiconductors produced by using either top-down or bottom-up approaches.

Keywords: nanowires, ion beam doping, flash lamp annealing

1. Introduction

Semiconducting nanowires (NWs) hold promises for functional nanoscale devices [1, 2]. The success of NWs ultimately depends on the possibilities of controlling their electrical, magnetic and optical properties through doping. Although several applications have been demonstrated in the areas of electronics, photovoltaics and sensing [1-4], the doping of NWs remains a challenging task. Typically, doping can be performed either i) in-situ [5, 6], taking place during growth, or ii) ex-situ [7, 8] via diffusion or ion implantation after growth.

Ion implantation is a standard doping method in semiconductor industry [9], which offers precise control over the areal dose and depth profile of nearly all elements of the periodic table even beyond their equilibrium solid solubility [10]. Yet its major disadvantage is the concurrent material damage. A subsequent annealing process is commonly used for the healing of implant damage and the electrical activation of dopants. This step, however, might lead to the segregation of dopants and eventually the degradation of NWs because of the low thermal stability caused by the large surface-area-to-volume ratio.

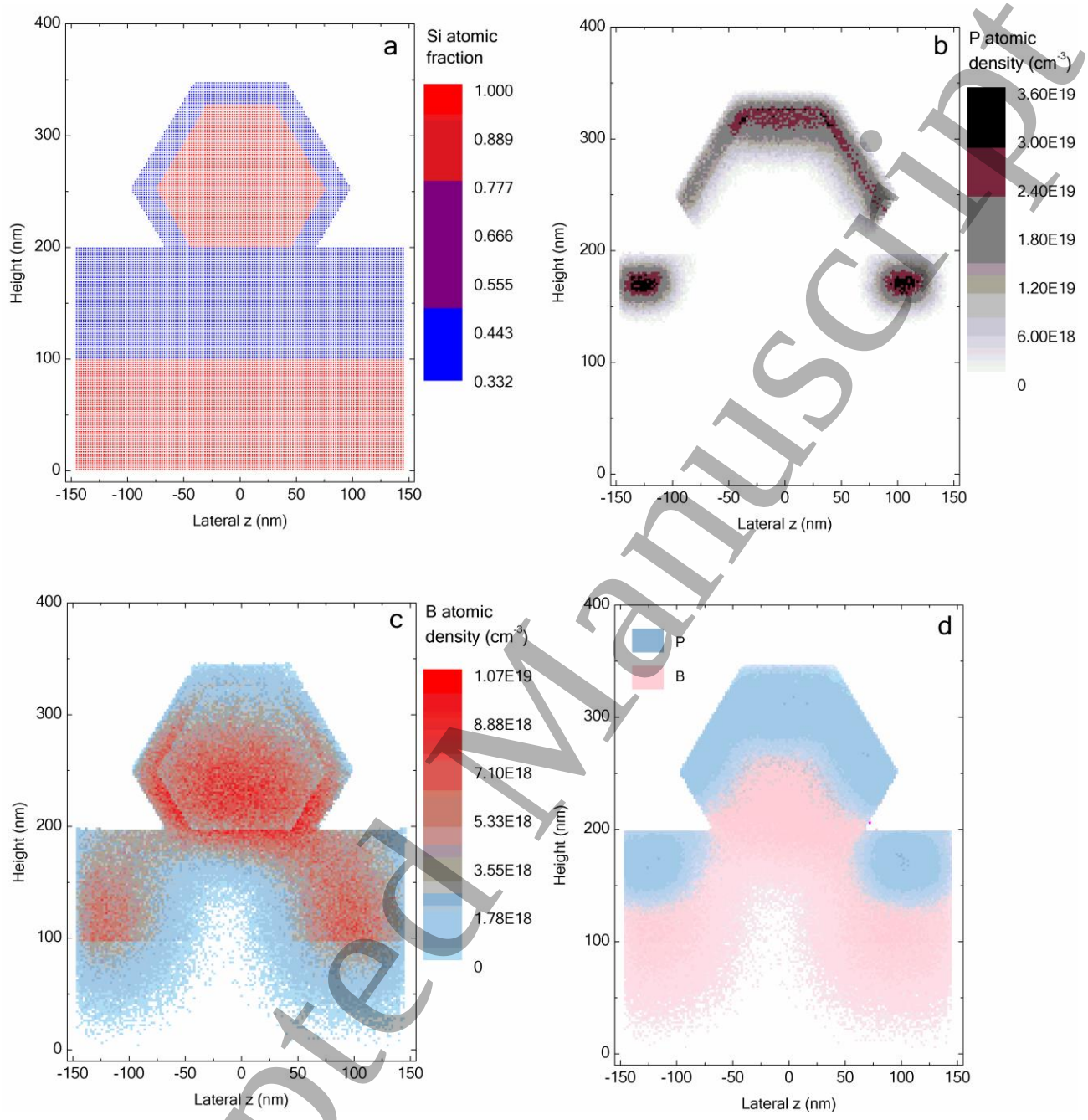

Figure 1. Cross-sectional view of dynamic Monte Carlo computer simulations results for P and B implantation into a Si/SiO_2 core/shell <111> oriented NWs (130nm diam. core/20nm SiO_2 shell) resting on SiO_2(100 nm)/Si substrate. The implantation energy is 20 keV, while the fluence is 1×10^{14} cm^{-2}. (a) Si atomic fraction of the Si/SiO_2 core/shell NW. (b) P atomic density profile in cm^{-3} (c) B atomic density profile in cm^{-3} and (d) Red-green-blue (RGB) plot of P- and B-implanted Si/SiO_2 core/shell NWs leading to the formation of the n- and p-type regions, respectively. Two-color representation of the P:B composition.

The ion beam doping of Si NWs using P and B has previously been tackled [11-14]. The low electrical activation and segregation of P and B dopants are reported to be the critical issues [12, 13]. Conventional annealing techniques under thermal equilibrium conditions such as furnace annealing are used resulting in a strong segregation of P and B dopants accompanied by a low electrical activation of both

elements [13]. These effects have been found to be even more accentuated when annealed in O_2 atmosphere, since during long-time thermal annealing the formation of an oxide layer at the surface of the NWs enhances the segregation of B and P at the Si/SiO_2 interface.

A possible solution to overcoming these issues might be a non-equilibrium thermal processing performed under an oxygen-poor annealing atmosphere, by which the diffusion length of dopants is controlled via the annealing time that has to be long enough to allow for the healing of the implanted region, but in turn sufficiently short to avoid the segregation of the implanted elements.

In this work, we report on the ion beam doping of individual drop-casted Si/SiO_2 core/shell NWs using conventional dopants via non-equilibrium processing. The approach is based on the implantation of P and B ions at different depths in the Si core followed by millisecond-range flash lamp annealing (FLA). Scanning spreading resistance microscopy (SSRM) measurements through a bevel formed along the NW enabled us to demonstrate the concurrent formation of n- and p-type regions in individual Si/SiO_2 core/shell NWs.

2. Modelling and experimental details

Ion beam doping of individual drop-casted Si/SiO_2 core/shell NWs was modelled by the three-dimensional dynamic computer simulation TRI3DYN [15]. Arbitrary 3D bodies can be arranged within a fixed cuboidal computational volume spanned by the Cartesian coordinates *x*, *y* and z, which is subdivided into fixed cuboidal voxels. For the present problem, an infinitely long wire is set up on a pedestal which represents the substrate, with the wire axis along the *y* direction and periodic boundary conditions in *y*. The *x* axis points from the top of the wire into the substrate. Laterally in *z* direction, open boundaries are applied to simulate the irradiation of a single isolated NW. The total extension of the computational volume is $x_{max} \times y_{max} \times z_{max} = 260\,nm \times 100\,nm \times 320\,nm$, so that the spatial extension of the collision cascade fits well into the system in *y* direction. The voxel spacing is $2\,nm \times 2\,nm \times 2\,nm$. Further details can be found elsewhere [15].

Room-temperature implantation of P and B ions was performed using the 40 kV ion implanter at the Ion Beam Center at Helmholtz-Zentrum Dresden-Rossendorf. The implantation parameters (energy and fluence) were determined using TRI3DYN.

μ-Raman spectroscopy was employed to determine the phonon spectra of individual NWs that were transferred onto Scotch tape to be used as a dummy substrate. This eliminated phonon contributions from the bare Si substrate. Spectra were obtained in the wavenumber range of 200 to 650 cm^{-1} with a resolution of approximately 0.1 cm^{-1}. The Raman scattering was excited with a 532 nm Nd:YAG laser, linearly polarized along the long axis of the NW, to optimize Raman signal intensity. The power of the laser was kept sufficiently low to avoid any shift in the phonon peaks arising from laser-induced heating. All the measured phonon spectra were corrected by the Raman spectrum of the Scotch tape.

Cross-sectional high-resolution transmission electron microscopy (TEM) investigations were performed with a Titan 80–300 microscope (FEI) operated at an accelerating voltage of 300 kV. TEM lamellae of NW cross-sections were prepared by in-situ lift-out using a Zeiss Crossbeam NVision 40 system. To protect the NW surface at the area of interest, a carbon cap layer was first deposited aided by the electron beam and followed by Ga-focused ion beam (FIB)-assisted precursor decomposition. Subsequently, the TEM lamella was prepared using a 30 keV Ga FIB with adapted currents and then transferred to a 3-post copper lift-out grid (Omniprobe) using a Kleindiek micromanipulator. For final thinning of the TEM lamella to electron transparency, low-energy (5 keV) Ga ions were employed at glancing incidence to minimize sidewall damage.

In order to determine the depth profile of the electrically active dopants in the NWs by SSRM, a bevel in an individual Si/SiO_2 core/shell NW was formed using electron beam lithography (EBL) and dry etching. First, the sample with the NWs was spin-coated with around 350 nm of the positive resist ZEP520A (Zeon Corp.). Then, a 50×50 μm^2 opening at one end of the selected NW was made in the resist by EBL. This step was followed by dry etching of the NW through the opening in an inductively coupled plasma (ICP) of SF_6 and C_4F_8. In this process, SF_6 acts as an etchant and C_4F_8 is responsible for sidewall passivation to enable anisotropic etching [16]. Etching parameters leading to the desired slope of the bevel were SF_6 and C_4F_8 gas flow: 12 sccm and 20 sccm, respectively, ICP power: 400 W, platen power: 12 W, pressure: 1.13 Pa. After etching, the ZEP520A layer was removed using ZDMAC (dimethylacetamide) remover (Zeon Corp.). Additionally, an ohmic contact at one of the NW edges is made for the SSRM measurements by EBL (Au deposition and lift-off). To ensure good contact quality, reactive ion etching is carried out to remove the SiO_2 shell at the contact part of the NW just before the Au metallization step.

SSRM investigations were performed using a Bruker multimode system working in contact mode and equipped with an application module for SSRM measurements. This allows for mapping the two-dimensional surface resistivity while simultaneously collecting topography data. A multimode TR-Tuna cantilever holder with a conductive diamond-coated AFM-tip was used. Gwyddion software was

employed for visualization and analysis of the experimental data.

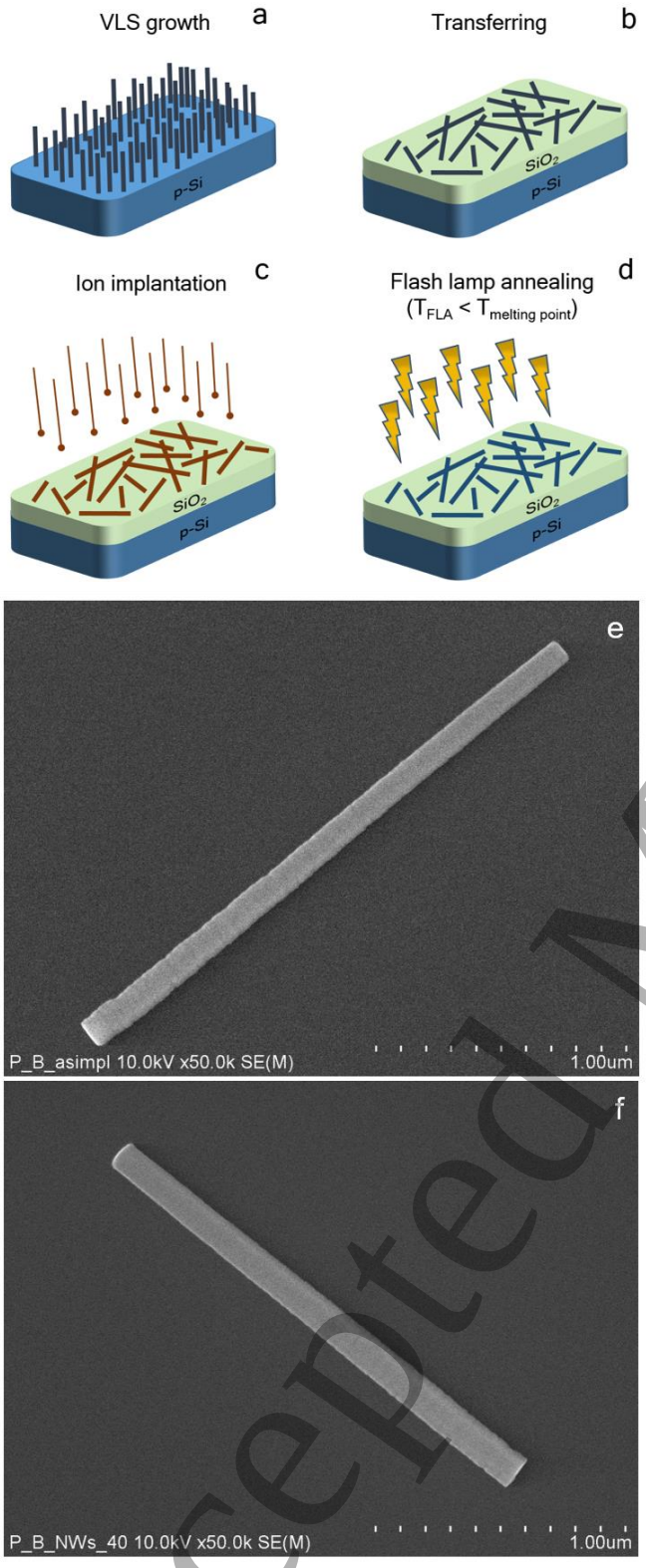

Figure 2. Schematic illustration of the non-equilibrium processing for the P and the B doping of Si/SiO_2 core/shell NWs. (a) Si/SiO_2 core/shell NWs vertically grown on a Si substrate by the VLS method followed by PECVD for the SiO_2 shell formation. (b) Transferred Si NWs via sonification in ethanol onto a 70-nm-thick SiO_2 insulating layer deposited on top of a p-type Si substrate. The drop-casted NWs are randomly oriented. (c) Room-temperature ion implantation process of B and P at different depths across the NW core. (d) Millisecond-range flash lamp annealing that ensures annealing temperatures below the melting point of amorphous Si (~1480 K) [19]. Representative top-down SEM images of (a) an individual as-implanted Si/SiO_2 core/shell NW and (b) an individual FL-annealed Si/SiO_2 core/shell NW.

3. Results and discussion

Three-dimensional dynamic Monte Carlo simulations were performed in order to determine the implantation parameters leading to the formation of cross-sectional n- and p-type doped regions in an individual drop-casted Si/SiO_2 core/shell NW. P and B ions are the dopants of choice for the n- and the p-type doping, respectively. The main results derived from the simulations are summarized in figure 1. In detail, figure 1(a) shows the cross-sectional view of the Si atomic fraction of a P- and B-implanted 150-nm Si core/20-nm SiO_2 shell NW resting on a 100-nm thick SiO_2 layer atop a Si substrate. The implantation energy and the fluence to implant P and B ions at different depths across the NW core with neither atom migration nor changes in the morphology of NWs are determined to be 20 keV and 1×10^{14} cm^{-2}, respectively. The SiO_2 shell was considered as a capping layer to adjust the implantation parameters. These parameters were also tailored to be below the amorphization threshold of both P and B in Si, which typically takes place upon high-fluence ion implantation. In the present Si/SiO_2 core/shell NW structure, the light B ions penetrate significantly deeper due to their low mass and atomic number and the associated lower stopping force. The peak P atomic density is localized in the top half of the NW core and the SiO_2 shell (figure 1(b)), while the peak B atomic density is centered at the middle-bottom half of the NW core (figure 1(c)). This results in the formation of a n-type doped region followed by a p-type doped region across the NW core (figure 1(d)).

Having determined the implantation parameters from simulations, the vapor-liquid-solid (VLS) growth mechanism is used to epitaxially grow Si NWs on <111> Si substrates [17]. The growth conditions are optimized to render as-grown <111> oriented NWs with a diameter ranging from 80 to 160 nm and an average length of around 7 μm (figure 2(a)). Si/SiO_2 core/shell NWs are then produced by depositing a 20 nm thick SiO_2 shell via plasma-enhanced chemical vapor deposition (PECVD). Subsequently, the Si/SiO_2 core/shell NWs are harvested by a sonication method in ethanol and drop-casted on 70 nm thick SiO_2 layer deposited by PECVD on top of a Si substrate (figure 2(b)). The drop-casted Si/SiO_2

core/shell NWs are then implanted with P and B ions at the same fluence of 1×10^{14} cm^{-2} and the same energy of 20 keV (figure 2(c)). As shown in figure 1, the dynamic Monte Carlo simulations predict that these parameters might lead to an atomic P distribution peak close to the upper half of the NW core, while the atomic B distribution peak ought to lie on the middle of the NW core. In order to electrically activate P and B atoms, to prevent the segregation of both dopants and to heal the concurrent material damage upon implantation, the implanted Si/SiO_2 core/shell NWs are then flash-lamp annealed in N_2 atmosphere at an energy of 73 J/cm^2 for 3 ms accompanied by a preheating at 300ºC for 30 s (figure 2(d)). Further details about FLA can be found elsewhere [18]. The integrity of the Si/SO_2 core/shell NWs upon the P and B implantation followed by FLA is verified by scanning electron microscopy (SEM) images (figure 2 (e) and (f)).

μ-Raman backscattering measurements were performed to investigate the crystalline quality of individual Si/SO_2 core/shell NWs and the activation of dopant atoms by FLA. A disorder in the crystalline structure of Si/SO_2 core/shell NWs is observed upon P and B implantation, in spite of the fact that the fluence was chosen to be below the amorphization threshold (figure 3). The 493 cm^{-1} peak related to the Si–Si vibrational modes for the as-implanted NWs accounts for the aforementioned disorder of the crystalline Si structure [20]. Alternatively, the implantation-related disorder in the crystalline structure of an individual Si/SO_2 core/shell NW is fully restored upon FLA. Apart from the well-resolved 520 cm^{-1} first-order optical phonon (TO_{Si}) and the 303 cm^{-1} second-order two transverse acoustic phonon ($2TA_{Si}$) scattering peaks, the ^{11}B local vibrational peak at around 618 cm^{-1} is also observed [12, 21, 22] (figure 3). This indicates that the B atoms are placed in Si substitutional sites in the crystalline Si core of the Si/SO_2 core/shell NW. Moreover, the room-temperature local vibrational mode of substitutional P in Si is known to be around 441 cm^{-1} [21]. Although a peak is not clearly resolved, it might be possible that substitutional P atoms are responsible for the weak broad kink spanning from 400 to 450 cm^{-1}.

The crystalline structure and morphology of as-implanted and FL-annealed Si/SO_2 core/shell NWs were inspected by high-resolution transmission electron microscopy. The formation of <111>-oriented Si/SiO_2 core/shell NWs by combining VLS and PECVD methods is confirmed in figure 4. Despite remaining single-crystalline structure of the NWs upon implantation of P and B atoms, a crystalline disorder is observed at the rim of the Si core (figure 4(a) and (c)). This is, however, restored after FLA where the single-crystalline nature of the NW is found to be evenly extended along the whole Si core (figure 4(b) and (d)). The millisecond-FLA also leads to a well-defined core/shell interface as observed in figure 4(d). These findings are in agreement with the Raman results shown in figure 3. In particular, the observed 493 cm^{-1} peak in the Raman spectrum of the as-implanted NW is cross-checked to be related to the Si–Si vibrational modes coming from the disordered crystalline rim of the Si core.

A top-view SSRM image of an individual P and B implanted Si/SiO_2 core/shell NW together with the Au contact is visualized in figure 5(a). This approach allows for measuring any change in the conductivity of the NW along the bevel, which is expected to be related to the n- and the p-type doped regions. The effectiveness of our method in producing a bevel along an individual P- and B-implanted Si/SiO_2 core/shell NW is evidenced by a topographic mapping derived from SSRM measurements (figure 5(b)). The bevel height as a function of projected bevel length reflects a change in the slope that is found to be correlated with the different etching rates in SiO_2, P- and B-doped Si (figure 5(c)). From the bevel profile, the thickness of both the P- and B-doped Si was estimated to be around 30 nm, which correlates well with the dopant profile derived by ion-implantation simulations (figure 1(b) and (c)). By scanning the AFM-tip over the bevel, the surface conductivity (electrical current distribution) as a function of projected bevel length is recorded (figure 5(c)). Different regions along the projected bevel length can be identified in which the surface conductivity changes. In case of the SiO_2 shell and the un-doped Si (the top and the bottom regions of the bevel, respectively), the conductivity remains constant at very low values. On the contrary, an abrupt increase of the conductivity in the P- and B-doped Si regions is observed for the projected bevel length of around 200-500 nm. In particular, a kink on the surface conductivity at the projected bevel length of around 400 nm accounts for the transition region between the n- and the p-doped regions. These results indicate the electrical activation of both dopants which in turn confirms the formation of n- and p-type regions by the implantation of P and B ions and the subsequent FLA.

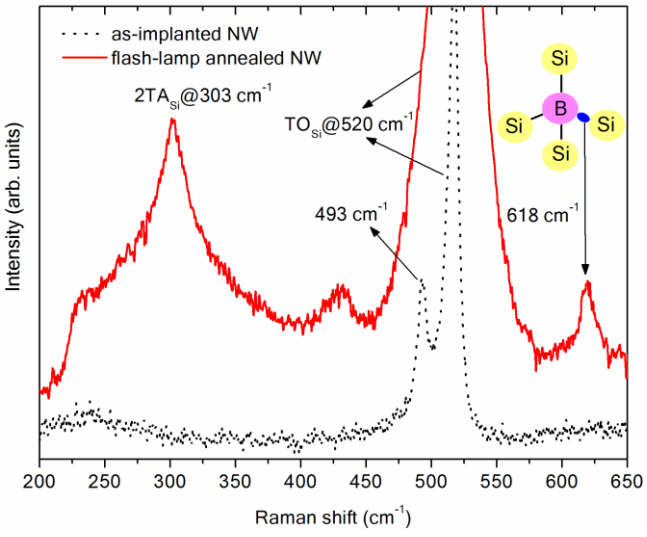

Figure 3. μ-Raman spectra for individual as-implanted and flash-lamp annealed Si/SO_2 core/shell NWs. B local vibrational peak observed for an individual NW after subsequent activation FLA.

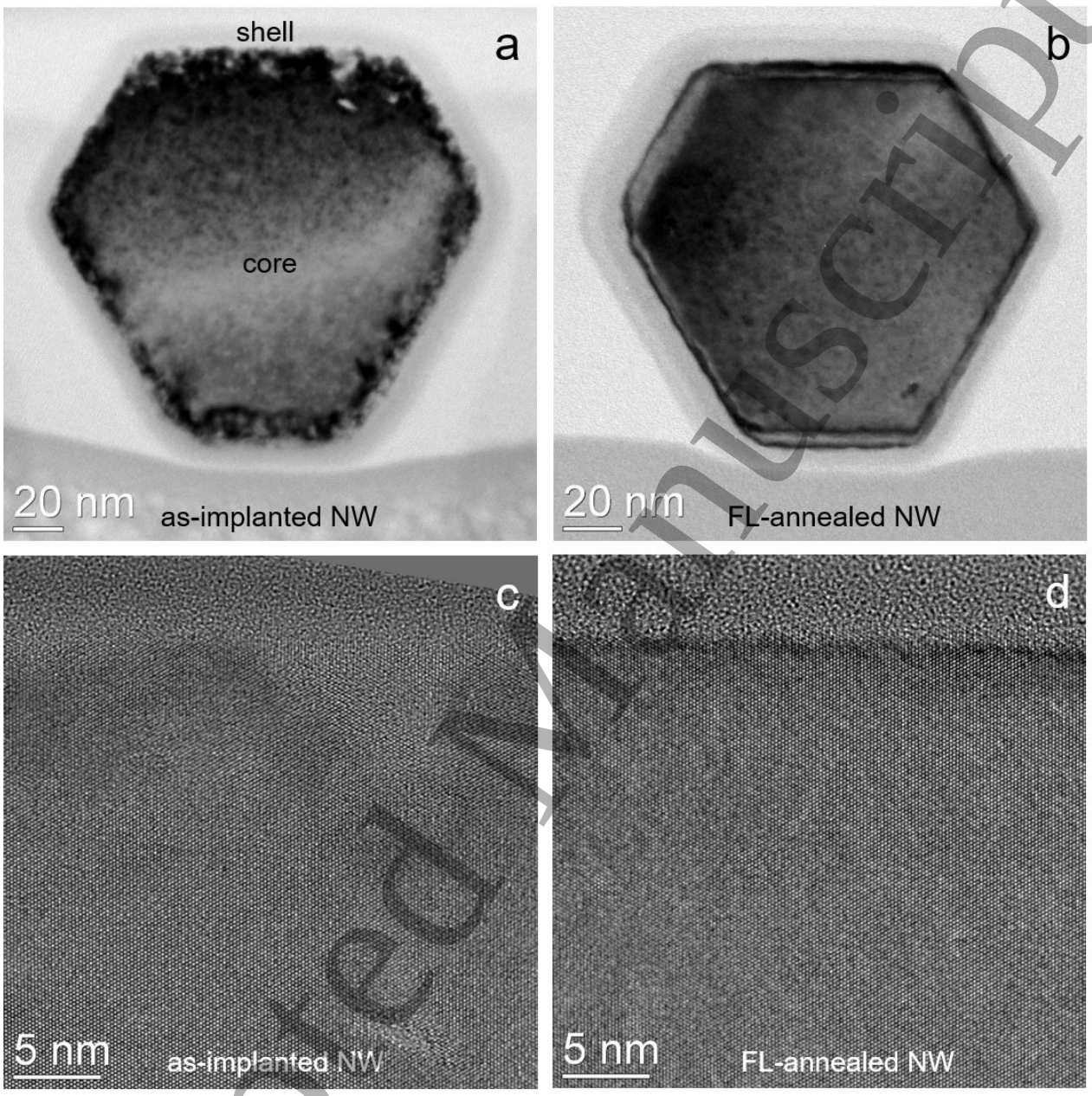

Figure 4. Cross-sectional bright-field TEM images of (a) as-implanted Si/SiO_2 core/shell NW and (b) FL-annealed Si/SiO_2 core/shell NW doped with P and B as well as representative cross-sectional high-resolution TEM images taken at the core/shell interface of (c) as-implanted NW and (d) FL-annealed NW.

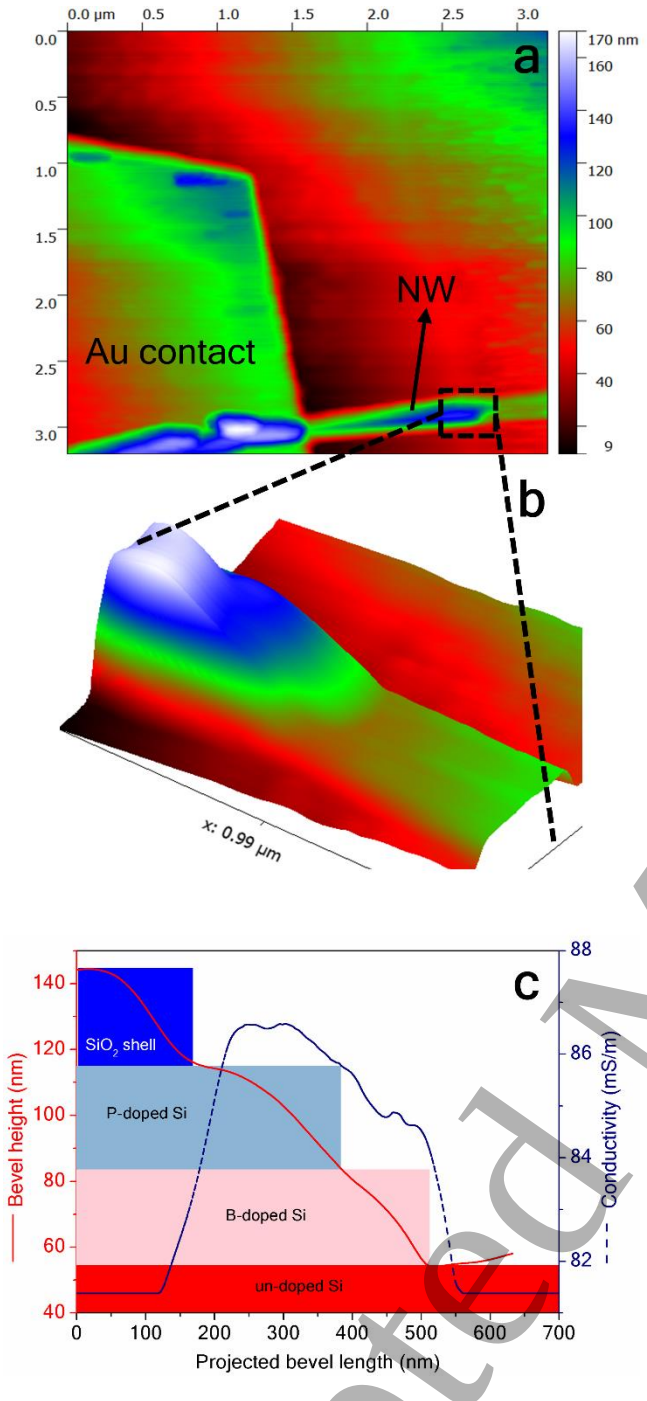

Figure 5. (a) A top-view image from SSRM of an individual P and B implanted Si/SiO_2 core/shell NW, where the black color corresponds to regions with minimum height, while the white color corresponds to regions with maximum height. (b) A topographic image of the formed bevel along the long axis of the individual P and B implanted Si/SiO_2 core/shell NW. (c) Bevel height (solid red curve) together with the measured conductivity (dashed navy curve) projected along the bevel length in an individual Si/SiO_2 core/shell NW as deduced from the SSRM measurements.

4. Conclusion

In conclusion, a method for the P and B doping of individual Si/SiO_2 core/shell NWs using ion implantation followed by millisecond-range flash lamp annealing has been demonstrated. This CMOS-compatible approach has been proven to be effective to heal the implantation-related damage and to electrically activate the implanted P and B dopants in silicon structures with nanometer-scale dimensions. These findings might unlock a route for controlled ion beam doping of nanostructured materials with the desired uniformity as well as control over the areal dose and profile of dopants.

Acknowledgements

Support by the Ion Beam Center at Helmholtz-Zentrum Dresden-Rossendorf in Germany is gratefully acknowledged. Y.B. would like to thank the Alexander-von-Humboldt foundation for providing a postdoctoral fellowship. The authors also thank Lothar Bischoff and Annette Kunz for the TEM lamella preparation of individual nanowires via focused ion beam milling.

References

[1] Cui Y, Lieber C M 2001 *Science* **291** 851.
[2] Colinge J P *et al.* 2010 *Nat. Nanotech.* **5** 225
[3] Beard M C, Luther J M and Nozik A J 2014 *Nat. Nanotechnol.* **9** 951
[4] Sadeghian R B, Islam M S 2011 *Nat. Mater.* **10** 135
[5] Schmid H, Björk M T, Knoch J, Karg S, Riel H and Riess W 2009 *Nano Lett.* **9** 173
[6] Gentile P, Solanki A, Pauc N, Oehler F, Salem B, Rosaz G, Baron T, Den Hertog M and Calvo V 2012 *Nanotechnology* **23** 215702
[7] Moselund K E *et al.* 2010 *Nanotechnology* **21** 435202
[8] Das Kanungo P, Kögler R, Nguzen-Duc K, Zakharov N, Werner P and Gösele U 2009 *Nanotechnology* **20** 165706
[9] Rimini E 1995 *Ion Implantation: Basics to Device Fabrication* (Boston: Kluwer Academic Publishers)
[10] Berencén Y *et al.* 2018 *Adv. Mater. Interfaces* **5** 1800101
[11] Colli A, Fasoli A, Ronning C, Pisana S, Piscanec S and Ferrari A C 2008 *Nano Lett.* **8** 2188
[12] Fukata N, Takiguchi R, Ishida S, Yokono S, Hishita S and Murakami K 2012 *ACS Nano* **6** 3278
[13] Fukata N, Ishida S, Yokono S, Takiguchi R, Chen J, Sekiguchi T and Murakami K 2011 *Nano Lett.* **11** 651
[14] Cui Y, Duan X, Hu J and Lieber C M 2000 *J. Phys. Chem. B* **104** 5213
[15] Möller, W 2014 *Nucl. Instrum. Methods Phys. Res., Sect. B* **322** 23
[16] Docker P T, Kinnell P and Ward M C L 2003 J. Micromech. Microeng. **13** 790
[17] Lugstein A, Steinmair M, Hyun Y J, Hauer G, Pongratz P and Bertagnolli E 2008 *Nano Lett.* **8** 2310
[18] Rebohle L, Prucnal S, Skorupa W 2016 *Semicond. Sci. Technol.* **31** 103001.

[19] Thompson M, Galvin G J, Mayer J W, Peercy P S, Poate J M, Jacobson D C, Cullis A G and Chew N G 1984 *Phys. Rev. Lett.* **52** 2360

[20] Jain K P, Shukla A K, Ashokan R, Abbi S C and Balkanski M, 1985 *Phys. Rev. B*, **32** 6688

[21] Barker A, Sievers A 1975 *Rev. Mod. Phys.* **47**, S1

[22] Fukata N, Chen J, Sekiguchi T, Okada N, Murakami K, Tsurui T and Ito S 2006 *Appl. Phys. Lett.* **89** 203109